

## A CENSUS OF BROAD-LINE ACTIVE GALACTIC NUCLEI IN NEARBY GALAXIES: COEVAL STAR FORMATION AND RAPID BLACK HOLE GROWTH

JONATHAN R. TRUMP,<sup>1</sup> ALEXANDER D. HSU,<sup>2</sup> JEROME J. FANG,<sup>1</sup> S. M. FABER,<sup>1</sup> DAVID C. KOO,<sup>1</sup> AND DALE D. KOCEVSKI<sup>1</sup>

*Draft version January 4, 2018*

### ABSTRACT

We present the first quantified, statistical map of broad-line active galactic nucleus (AGN) frequency with host galaxy color and stellar mass in nearby ( $0.01 < z < 0.11$ ) galaxies. Aperture photometry and  $z$ -band concentration measurements from the Sloan Digital Sky Survey (SDSS) are used to disentangle AGN and galaxy emission, resulting in estimates of uncontaminated galaxy rest-frame color, luminosity, and stellar mass. Broad-line AGNs are distributed throughout the blue cloud and green valley at a given stellar mass, and are much rarer in quiescent (red sequence) galaxies. This is in contrast to the published host galaxy properties of weaker narrow-line AGNs, indicating that broad-line AGNs occur during a different phase in galaxy evolution. More luminous broad-line AGNs have bluer host galaxies, even at fixed mass, suggesting that the same processes that fuel nuclear activity also efficiently form stars. The data favor processes that simultaneously fuel both star formation activity and rapid supermassive black hole accretion. If AGNs cause feedback on their host galaxies in the nearby universe, the evidence of galaxy-wide quenching must be delayed until after the broad-line AGN phase.

*Subject headings:* galaxies: active — galaxies: nuclei

### 1. INTRODUCTION

The well-studied correlations between supermassive black hole (SMBH) mass and properties of the host galaxy bulge (e.g., Magorrian et al. 1998; Gebhardt et al. 2000; Ferrarese & Merritt 2000; Marconi & Hunt 2003) indicate that SMBH growth may be intimately tied to galaxy evolution. However the causal physics behind the SMBH-galaxy link remains mysterious. Theoretical simulations suggest that rapidly accreting SMBHs in the active galactic nucleus (AGN) phase correspond to periods of recent massive star formation in their host galaxies (e.g., Hopkins et al. 2006, 2008). Powerful AGNs may also cause “feedback” on their host galaxies, shutting down star formation by blowing out the star-forming gas either via radiative winds (Silk & Rees 1998; Fabian 2002; Di Matteo, Springel, & Hernquist 2005) or radio jets (Croton et al. 2006). Observational evidence for star formation or feedback coevolving with black hole growth can be found in the star formation histories of AGN host galaxies (e.g., Heckman & Kauffmann 2006).

Of particular interest are the hosts of the most luminous AGNs, which are readily identified by broad emission lines in their optical spectra (e.g., Vanden Berk et al. 2001). These broad-line AGNs rapidly accrete material at rates of 1% to 100% of the Eddington limit (Kollmeier et al. 2006; Trump et al. 2009), and so require plentiful gas in their hosts, with the possibility of accompanying star formation activity. There is also evidence that broad-line AGNs universally have high velocity optical and X-ray outflows (Ganguly & Brotherton 2008; Winter 2010), indicative

of powerful winds and the potential for effective feedback in shutting down star formation. Studying the mass and rest-frame color of the host galaxy can reveal its recent star formation history: at a given stellar mass, galaxies that are very blue in rest-frame  $u-z$  have recently experienced a great deal of star formation, while red galaxies are quiescent and dominated by old stars. However the brightness of many broad-line AGNs complicates observations of their host galaxies, since the AGN often outshines the galaxy’s starlight.

Most authors simply avoid the problem of AGN contamination by studying host-dominated AGN. “Host-dominated” means that the accreting black hole is either obscured or weakly accreting (Eddington ratios of  $< 1\%$ ), and the photometry is dominated by the host galaxy. Studies of such host-dominated AGNs suggest a preference for massive ( $\log(M_*/M_\odot) > 10.5$ ) host galaxies (Kauffmann et al. 2003b; Haggard et al. 2010), although Aird et al. (2012) suggest this is a relic of selection effects and AGNs are instead equally likely to be in hosts of any stellar mass. Several observations suggest that host-dominated AGNs are most often found in “green valley” galaxies, so-called because they have colors intermediate between the more densely populated star-forming blue cloud and the passive red sequence of galaxies (Nandra et al. 2007; Salim et al. 2007; Georgakakis et al. 2008; Silverman et al. 2008; Gabor et al. 2009; Schawinski et al. 2009; Hickox et al. 2009; Kocevski et al. 2009). Other studies, however, argue that active galaxies have the same color distribution as inactive galaxies of similar mass and the apparent green valley peak for AGN hosts is caused only because AGNs prefer massive galaxies (Silverman et al. 2009; Xue et al. 2010). Cardamone et al. (2010) additionally argue that the apparent green valley hosts of AGNs are just dust-reddened star-forming (and intrinsically blue) galaxies, and dust-corrected AGN hosts have

<sup>1</sup> University of California Observatories/Lick Observatory and Department of Astronomy and Astrophysics, University of California, Santa Cruz, CA 95064 USA

<sup>2</sup> The Harker School, 500 Saratoga Avenue, San Jose, CA 95129 USA

the same color distribution as inactive galaxies.

Besides the difficulties in the differing interpretations, the above studies include only obscured or weakly accreting AGNs with very different fueling and outflow properties from luminous broad-line AGNs (Ho 2008; Trump et al. 2011). By definition, host-dominated AGNs do not dominate the energetics of their hosts, and probably have minimal influence on the current star formation in their galaxies. Studying the impact of AGNs on galaxy evolution requires observing galaxies during the most rapid period of SMBH growth.

Studies of broad-line AGN host galaxies have generally used structural decomposition of high spatial resolution *Hubble Space Telescope* (*HST*) images (e.g., Peng et al. 2002). By modeling the luminous point-source AGN and subtracting it from the extended host galaxy light, the intrinsic galaxy properties can be disentangled from the contaminating AGN. The first high-resolution studies of quasar hosts suggested that these luminous AGNs prefer massive and luminous hosts (Bahcall et al. 1997). The host galaxies of luminous AGNs were also found to have younger stellar populations than inactive galaxies of the same mass, with colors spanning the blue cloud and green valley (Jahnke et al. 2004a,b). However the need for high-resolution *HST* imaging limited these studies to small numbers ( $\sim 20$ ) of AGNs. Recent Herschel far-infrared studies, also limited to small samples, similarly suggest that more luminous AGNs have higher star formation rates than their inactive counterparts (Santini et al. 2012; Rovilos et al. 2012; but see also Mullaney et al. 2012).

In this work we expand host galaxy studies of rapidly accreting AGNs using 820 broad-line AGNs at  $0.01 < z < 0.11$  from the Sloan Digital Sky Survey. The large number of AGNs, with a set of matched inactive galaxies, allows for the first statistical map of broad-line AGN frequency across the nearby galaxy color-mass diagram. The selection and properties of the data are described in Section 2. Our AGN/host decomposition method is described in Section 3, which introduces a novel aperture photometry method for separating point-source AGNs and extended inactive galaxies. Section 4 reveals that broad-line AGNs have a strong preference for star-forming galaxies, and demonstrates that this preference is not a function of selection effects. We discuss what these results mean for the relationship between nuclear activity and star formation, and the efficacy of AGN feedback, in Section 5.

Throughout this work we assume a cosmology with  $h = 0.70$ ,  $\Omega_M = 0.3$ ,  $\Omega_\Lambda = 0.7$ .

## 2. OBSERVATIONAL DATA

We select samples of broad-line AGNs and inactive galaxies from the Sloan Digital Sky Survey (SDSS, York et al. 2000). Each type is selected using the spectroscopic classification provided by the SDSS DR7: broad-line AGNs are identified by *SpecClass*= 3, while galaxies without broad emission lines have *SpecClass*= 2. We visually inspected the spectra of all broad emission line AGNs to ensure they are correctly classified (removing the misclassified  $\sim 1\%$  of objects). Note that we refer to all galaxies without broad lines as inactive, while some of these “inactive” galaxies may actually have emission line ratios that suggest weak

or obscured AGNs (Baldwin, Phillips & Terlevich 1981; Kewley et al. 2006).

Given the parent sample of broad-line AGNs and inactive (non-broad-line) galaxies in the SDSS, we make the following cuts:

1. Face-on systems only, with  $b/a > 0.5$  (where  $b/a$  is the ratio between the minor and major axes of the  $r$ -band image). This constraint is designed to eliminate dusty systems and removes a significant number (36%) of inactive galaxies but only 15% of the initial broad-line AGNs.<sup>3</sup>
2.  $0.01 < z < 0.11$ . The sample is further sub-divided into  $\Delta z = 0.01$  bins (i.e.,  $0.01 < z < 0.02$ ,  $0.02 < z < 0.03$ , etc.) for the AGN light correction, as described in Section 3.
3.  $r < 17.77$ . This is the spectroscopy limit for inactive galaxies in the SDSS. Although the SDSS spectroscopy includes broad-line AGNs to fainter magnitudes ( $i < 19.1$  or  $i < 20.2$ ), we require  $r < 17.77$  for both samples to ensure a complete control sample.

The SDSS spectroscopy is  $>95\%$  complete to both galaxies and quasars in these redshift and magnitude ranges (Strauss et al. 2002; Richards et al. 2002). These initial selection criteria result in a total of 192,946 inactive galaxies and 972 broad-line AGNs. Beyond the redshift and magnitude limits, the sample is divided into luminosity-limited “faint” and “luminous” samples, each complete to a given  $r$ -band absolute magnitude.

- Luminous sample: This is limited to all  $0.01 < z < 0.11$  sources with  $M'_r < -20.8$ , which corresponds to the  $r < 17.77$  spectroscopy limit at  $z = 0.11$ . The luminous sample probes the full redshift range of the sample, and includes 769 broad-line AGNs and 110,670 inactive galaxies.
- Faint sample: This is limited to all  $0.01 < z < 0.05$  sources with  $M'_r < -19$ , which similarly corresponds to the  $r < 17.77$  limit at  $z = 0.05$ . The faint sample is designed to probe a large range of luminosities and stellar masses, with 134 broad-line AGNs and 33,361 inactive galaxies.

Note that galaxies in the faint sample with  $M'_r < -20.8$  are also in the luminous sample, and there are a total of 820 unique broad-line AGNs in the two samples.

### 2.1. Photometry

The SDSS provides magnitudes in five *ugriz* filters for all broad-line AGNs and inactive galaxies. We use both the total magnitude  $m$  integrated across the entire galaxy<sup>4</sup>, and the inner aperture magnitude  $m_{in}$  mea-

<sup>3</sup> The high  $b/a$  preference for broad-line AGNs could be a selection bias, such that a point source is biasing the axis ratio measurement. However several studies also suggest a genuine preference for broad-line AGNs to lie in spheroid-dominated (Bahcall et al. 1997) or face-on (Rigby et al. 2006) galaxies.

<sup>4</sup> Total magnitude  $m$  is the SDSS “model magnitude.” These magnitudes are computed over the same aperture in all five filters, with the aperture size computed from the model fit to the  $r$  band.

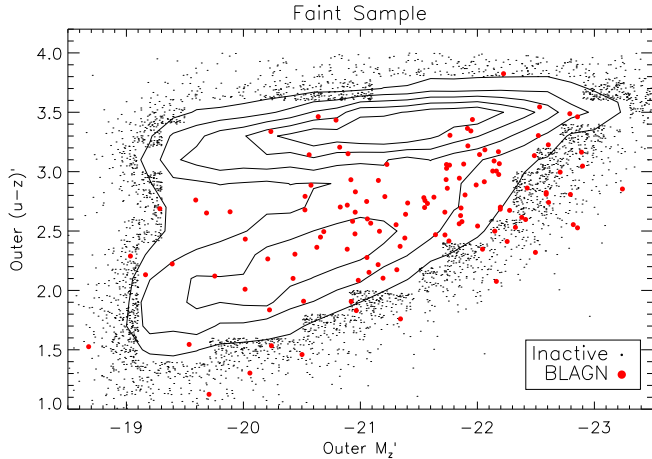


FIG. 1.— Outer  $(u-z)'$  color with outer  $M_z'$  absolute magnitude, each K-corrected to  $z = 0.05$ , for both inactive galaxies (contours and points) and broad-line AGNs (filled red circles) in the faint sample. Outer magnitudes represent the light outside a  $3''$  diameter aperture. Broad-line AGNs lie all over the color-magnitude diagram but tend to appear brighter and bluer than inactive galaxies because the AGN light contaminates even the outer magnitude measurements. Section 3 outlines the derivation and application of a correction that recovers the uncontaminated host galaxy light for broad-line AGNs.

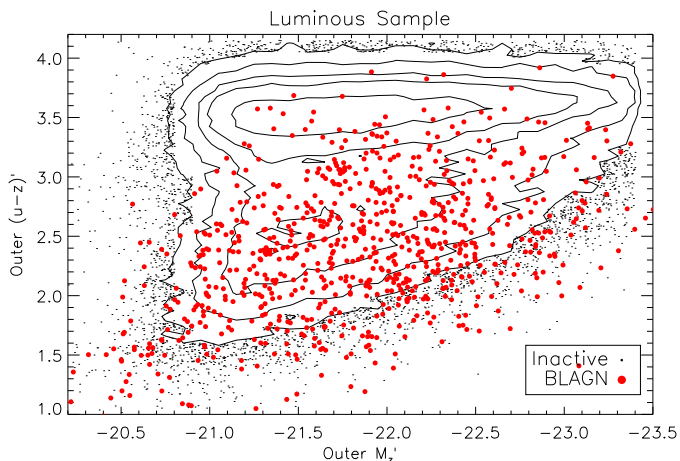


FIG. 2.— K-corrected outer  $(u-z)'$  color with outer  $M_z'$  absolute magnitude for the luminous sample, where outer magnitudes are defined as the light outside a  $3''$  diameter aperture. As in Figure 1, light from the AGN causes their hosts to appear brighter and bluer than inactive galaxies. The contaminating blue AGN light is particularly evident in the many AGNs with total  $M_r' < -20.8$  but outer  $M_z' > -20.8$  (in contrast to the typically redder inactive galaxy population).

sured within a  $3''$  diameter of the galaxy center<sup>5</sup>. An outer aperture magnitude  $m_{out}$  is calculated from the light outside the  $3''$  diameter, given by

$$m_{out} = -2.5 \log(10^{-0.4m} - 10^{-0.4m_{in}}). \quad (1)$$

Note that  $m_{in}$  is calculated after convolving the image to  $2''$ , which ensures uniform seeing for all objects. While convolving to lower resolution slightly worsens AGN contamination, it actually helps our AGN/galaxy decomposition by ensuring that all active galaxies have the same

<sup>5</sup> The inner aperture magnitude is not to be confused with the SDSS spectroscopic fiber magnitude:  $m_{in}$  is measured from the same photometric image as  $m$ .

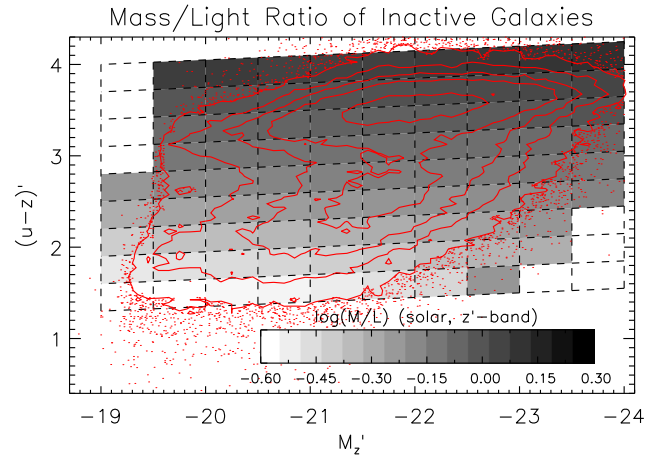


FIG. 3.— Median mass-to-light ratio, in the  $z'$ -band, for all inactive galaxies with  $r < 17.77$  at  $0.01 < z < 0.11$ . Mass-to-light ratio is computed in bins of color  $(u-z)'$  and luminosity ( $M_z'$ ), with no data shown for bins containing fewer than 5 galaxies. Mass-to-light ratio is a strong function of color and a weak function of luminosity. This figure is used to estimate masses for broad-line AGN hosts, using their corrected (AGN-subtracted) galaxy colors and luminosities to determine the appropriate mass-to-light ratio.

$2''$  resolution as the point-source stars and inactive galaxies used to calibrate the method.

We K-correct the observed photometry in both samples to the  $z = 0.05$  frame using the public `kcorrect` IDL software (Blanton & Roweis 2007). The prime ( $'$ ) notation is used to denote colors and magnitudes K-corrected to  $z = 0.05$ . Figure 1 shows the K-corrected outer  $(u-z)'$  color with the outer  $M_z'$  absolute magnitude for inactive galaxies and broad-line AGNs in the faint sample, and Figure 2 similarly shows the luminous sample. Naively one might assume that the outer magnitudes do not contain any light from the AGN point source. However both figures show that many broad-line AGNs have brighter and bluer outer magnitudes than the inactive galaxy population. Light from the SDSS point spread function (PSF) extends beyond the inner  $3''$  aperture, and a more sophisticated process is necessary to recover the uncontaminated galaxy properties. This technique is derived and applied in Section 3.

## 2.2. Stellar Masses

Galaxy stellar masses come from the MPA-JHU value-added catalog, derived according to Kauffmann et al. (2003a). Derived masses for the inactive galaxies have  $1\sigma$  errors of  $\sim 0.05$  dex, with no error dependence on mass or magnitude. However most of the broad-line AGN hosts are absent from this catalog, and those included in the catalog probably have inaccurate stellar masses due to the AGN contamination. To estimate masses for AGN hosts, we first calculate the mass-to-light ratios of inactive galaxies as a function of color and luminosity.

Figure 3 shows the median  $z'$ -band mass-to-light ratio in bins across the color-magnitude diagram. We use this figure to estimate masses for broad-line AGN hosts, applying the mass-to-light ratio from the bin corresponding to their corrected (AGN-subtracted) host galaxy color and absolute magnitude.

## 3. DISENTANGLING AGN AND GALAXY LIGHT

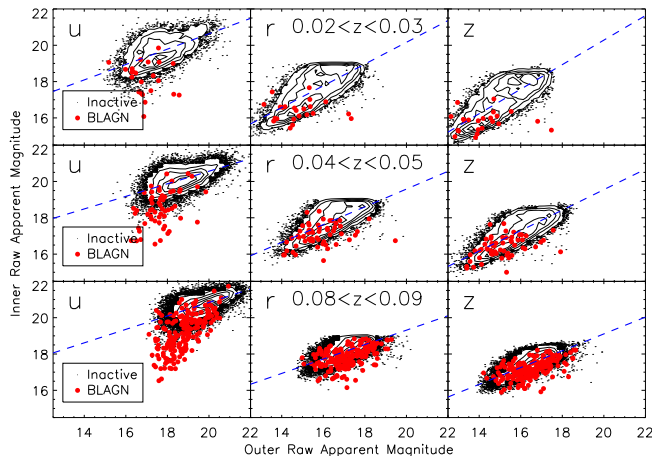


FIG. 4.— Inner vs. outer magnitudes for inactive galaxies (black contours and points) and broad-line AGNs (filled red circles) in three different filters and redshift ranges. The dashed blue line shows the best-fit line to the inactive galaxy population. Galaxies are typically fainter in  $u$  and  $r$  than  $z$ , and more distant galaxies appear fainter in their outer magnitudes (as their smaller apparent sizes cause more light to fall in the inner aperture). Broad-line AGN hosts typically have brighter inner magnitudes, particularly in blue light. The brightest AGNs additionally have slightly brighter outer magnitudes than inactive galaxies, as some AGN light “leaks” beyond the inner aperture and contaminates the outer aperture light (especially in the  $u$  band). The offset of a galaxy from the best-fit line is the residual  $\Delta m$  in Equation 2.

Broad-line AGNs dominate the light in the inner ( $<3''$ ) aperture but also contribute light in the outer ( $>3''$ ) aperture (as shown by Figures 1 and 2). We seek to remove the AGN emission to obtain uncontaminated measurements of host galaxy light. It turns out that inactive galaxies, uncontaminated by AGN light, have fairly tight relationships between  $z$ -band concentration and inner and outer magnitudes in each filter: we exploit these relationships to predict the galaxy-only magnitudes of AGN hosts. Likewise the relationship between inner and outer magnitudes of stars can predict the magnitudes of the AGN-only point-source component.

### 3.1. Galaxy Inner and Outer Aperture Magnitudes

We begin by comparing the inner ( $<3''$ ) and outer ( $>3''$ ) aperture magnitudes of inactive galaxies and broad-line AGNs. Figure 4 shows inner and outer magnitudes in three different filters ( $u$ ,  $r$ ,  $z$ ) and redshift ranges ( $0.02 < z < 0.03$ ,  $0.04 < z < 0.05$ ,  $0.08 < z < 0.09$ ). Light from broad-line AGNs has the strongest contaminating effect in blue light and inner magnitudes, but also affects outer magnitudes. For each of the five filters and in ten bins of redshift ( $0.01 < z < 0.11$  in  $\Delta z = 0.01$  intervals), we find the best-fit line describing outer ( $m_{out,GAL}$ ) and inner magnitude ( $m_{in,GAL}$ ) for inactive galaxies (shown by the dashed lines for the filters and redshift ranges in Figure 4). The offset above this line is defined by:

$$\Delta m = A + Bm_{out,GAL} - m_{in,GAL}. \quad (2)$$

The best-fit line is given by  $\Delta m = 0$ , and broad-line AGNs typically have  $\Delta m > 0$ . However even inactive galaxies have a large scatter in  $\Delta m$ , presumably because there is significant structural variation in galaxies of a given outer apparent magnitude. Adding a structural measurement could better describe the typical relation-

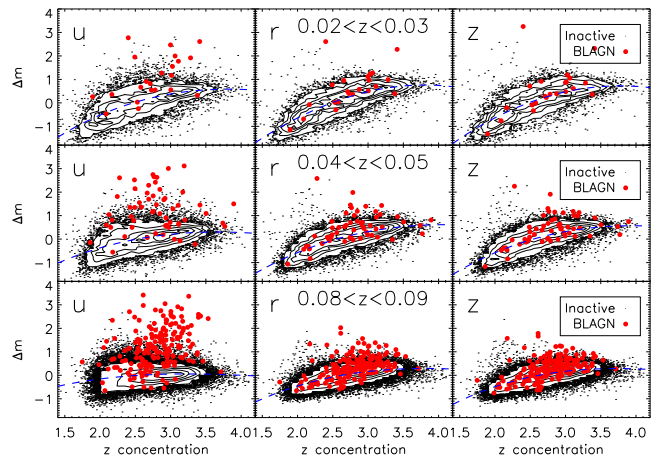


FIG. 5.— Offset from the best-fit line describing inner and outer magnitudes in Figure 4 ( $\Delta m$ , given by Equation 2) versus  $z$ -band concentration ( $C_z$ ) for inactive galaxies (black contours and points) and broad-line AGNs (filled red circles). The panels show the same three filters and redshift ranges as in Figure 4. The dashed blue line shows the best-fit cubic line to the inactive galaxy population. Broad-line AGNs have the same range in  $C_z$  as inactive galaxies, but tend to have significantly higher  $\Delta m$  (especially in blue light). The offset from the best-fit line is the residual  $\delta m$  in Equation 3.

ship for inner and outer magnitudes in inactive galaxies and explain their scatter about  $\Delta m = 0$ . In particular we use  $z$ -band concentration, defined as the ratio between the radius containing 90% of the  $z$ -band light and the radius containing 50% of the light,  $C_z = R_{90,z}/R_{50,z}$ .

Figure 5 shows  $\Delta m$  from Equation 2 versus  $z$ -band concentration  $C_z$ . Galaxies with  $\Delta m < 0$  (from fainter inner magnitudes than the average given their outer magnitude) have low concentration, while galaxies with  $\Delta m > 0$  (and brighter inner magnitudes) are more concentrated. The inactive population shows a tighter relation after using  $C_z$  to describe the structural variation, and broad-line AGNs scatter to brighter inner magnitudes and higher  $\Delta m$ .

A cubic line is fit to the inactive galaxies in Figure 5 (shown by the dashed line), with the offset from this line given by:

$$\delta m = \Delta m - C - DC_z - EC_z^2 - FC_z^3. \quad (3)$$

Figure 6 shows  $\delta m$  with  $C_z$  for inactive galaxies and AGNs. Broad-line AGN hosts tend to have  $\delta m > 0$ , as the AGN light causes the inner aperture magnitude to be brighter than expected given the galaxy’s  $z$  concentration. Inactive galaxies have  $\delta m \sim 0$  with small scatter: the standard deviation is typically only  $\sigma_{\delta m} = 0.3$  mag, with slightly larger  $\sigma_{\delta m} = 0.5$  mag scatter for low-concentration ( $C_z < 2.5$ ) galaxies in the  $u$  band. We use  $\delta m$  as an estimate of the brightness excess in the inner aperture due to AGN light.

Using Equation 3 for AGN/host decomposition has two important assumptions. First, we assume that  $C_z$  is not contaminated by the broad-line AGN. We originally chose  $C_z$  with this in mind:  $z$  band light is the least affected by the (typically blue) AGN, and  $R_{50}$  and  $R_{90}$  are large radii well beyond the point-source AGN. Figure 7 directly tests if the AGN affects  $C_z$  by plotting AGN luminosity against  $z$ -band concentration and comparing the distributions of  $C_z$  among broad-line AGNs and inactive galaxies. In general, both the faint and

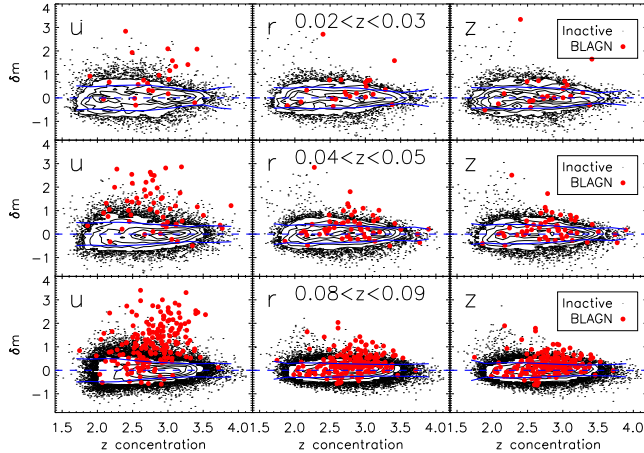


FIG. 6.— Offset from the best-fit cubic describing galaxy structure in Figure 5 ( $\delta m$ , given by Equation 3) versus  $z$ -band concentration ( $C_z$ ) in the same filters and redshift ranges as in Figures 4 and 5. Inactive galaxies are shown by black contours and points and broad-line AGN hosts are given by filled red circles. The dashed blue line shows  $\delta m = 0$ , and the solid blue lines show the scatter of the inactive galaxies about  $\delta m = 0$ .

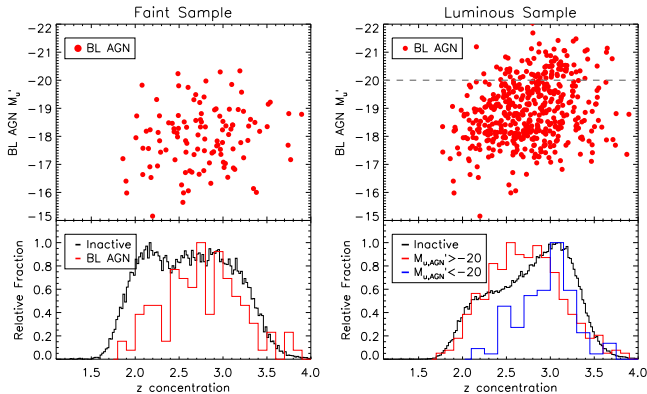


FIG. 7.— At top, the host-subtracted AGN  $u$ -band absolute magnitude with  $z$ -band concentration for both the faint ( $M'_u < -19$ ,  $0.01 < z < 0.05$ ) and luminous ( $M'_u < -20.8$ ,  $0.01 < z < 0.11$ ) samples. The bottom panels show histograms of the  $C_z$  distributions for both inactive galaxies and broad-line AGNs in both samples. The distribution of concentration among the most luminous ( $M'_{u,AGN} < -20$ ) AGNs peaks at higher values: we flag these high-luminosity AGNs in the subsequent discussion because their concentration might be biased by AGN contamination. Note that the different concentration distributions between the two inactive galaxy samples is caused by the luminous sample containing a higher proportion of high-mass spheroids than the faint sample.

luminous AGN samples span a wide range of concentrations. However the most luminous ( $M'_{u,AGN} < -20$ ) AGNs are typically more concentrated: this may be evidence that very luminous AGNs contaminate the concentration measurement, or it may be that more luminous AGNs prefer more bulge-like hosts (Bahcall et al. 1997; Cisternas et al. 2011; Kocevski et al. 2012). In case it is the result of a bias, we flag these high-luminosity AGNs when discussing any connections between AGN strength and host galaxy properties. Meanwhile we conclude that our assumption that  $C_z$  is unaffected by the AGN remains valid for the bulk of broad-line AGNs with  $M'_{u,AGN} > -20$ .

The second assumption is that all inactive galaxies

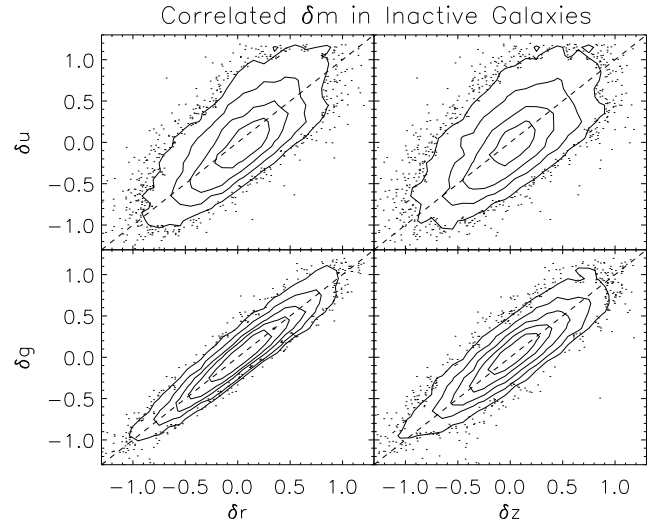


FIG. 8.— Comparisons of measured  $\delta m$  (from Equation 3) for inactive galaxies in  $ugrz$  filters. Values of  $\delta m$  in different filters are strongly correlated near the dashed one-to-one line.

have  $\delta m \sim 0$  with some random scatter  $\sigma_{\delta m}$ , independent of the presence of an AGN. There is evidence that this scatter is not due to measurement error: as Figure 8 shows, inactive galaxies have values of  $\delta m$  that are correlated across the  $ugriz$  filters. In other words, an inactive galaxy with  $\delta m \sim 1$  in the  $u$  band will also tend to have  $\delta m \sim 1$  in  $g, r, i, z$ . (This effectively means that the  $\delta m = 0$  assumption causes a much smaller scatter in color than in luminosity or stellar mass: see Section 3.4.) We tested if, in addition to  $C_z$ ,  $\delta m$  was connected to galaxy properties like color or Sérsic (1968) index. However we found no additional correlation and were unable to find the physical basis for the small scatter of inactive galaxies about  $\delta m = 0$ . Defining  $\delta m$  using color and Sérsic index instead of  $C_z$  also proved ineffective at reducing the scatter. Instead  $\sigma_{\delta m}$  is treated as a random error, and we investigate its effects in Section 3.4.

Inactive galaxies with  $\delta z > 1$  (in the upper left of the right panels in Figure 6) are potentially interesting because they have similar relationships between inner and outer magnitudes to bright AGNs. However after visually inspecting their images and spectra we determined that these galaxies probably have nuclear starbursts and are not some class of misclassified broad-line AGNs.

### 3.2. Point Source Inner and Outer Aperture Magnitudes

Most of the light from a point source is detected in the inner aperture, but the PSF of the SDSS causes light from point sources to “leak” into the outer aperture as well. Stars can be used to model the relationship between inner and outer aperture magnitudes for AGN-only light ( $m_{in,AGN}$  and  $m_{out,AGN}$ ), since both are point sources. We select a sample of 362 stars with  $r < 16$  and  $-0.2 < r - z < -0.1$ . The brightness ensures their photometry is well-measured, and the color cut makes them similar to the colors of bright AGNs.

Figure 9 shows the inner and outer magnitudes for the sample of 362 stars. These point sources have a well-defined relationship between inner and outer aperture magnitude, and the best-fit line in each filter describes the relationship between inner and outer magnitude for

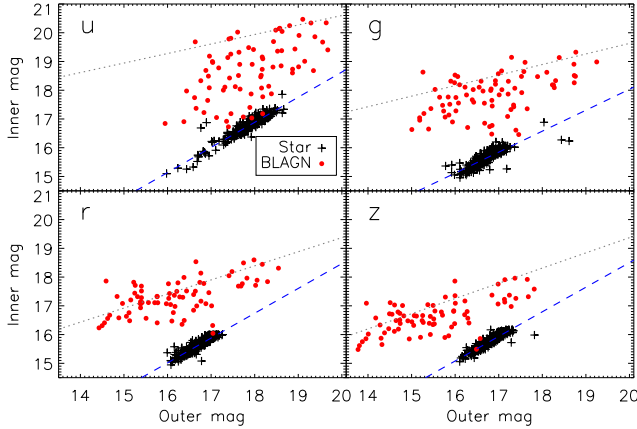


FIG. 9.— Inner and outer magnitudes in the *ugrz* filters for stars (black crosses) and broad-line AGNs at  $0.05 < z < 0.06$  (red circles). The blue dashed line in each panel shows the best-fit line for point-source stars, while the dotted gray line shows the best-fit line for  $0.05 < z < 0.06$  inactive galaxies (not shown). Broad-line AGNs tend to scatter between the two lines, with the brightest AGNs behaving like point sources (especially in *u*), and more modest AGNs behaving like inactive galaxies (especially in *r* and *z*).

the AGN-only light:

$$m_{in,AGN} = G + Hm_{out,AGN}. \quad (4)$$

Figure 9 shows that the brightest AGNs behave like point sources in blue light and lie on this line, while in red light AGNs behave more like inactive galaxies. Because all the images are convolved to  $2''$  before measuring the aperture photometry,  $m_{in,AGN} \approx 1 + m_{out,AGN}$  in all five filters.

### 3.3. The Equations for Decomposing AGN and Galaxy Light

Given the derived relationships between inner and outer magnitudes for galaxy-only (Equations 2 and 3) and AGN-only (Equation 4) light, we can solve for the unknown quantities  $m_{in,AGN}$ ,  $m_{out,AGN}$ ,  $m_{in,GAL}$ , and  $m_{out,GAL}$ . First, the total outer and inner magnitudes (both measured quantities) are simply the sum of the flux contributions from the AGN and the galaxy:

$$f_{in} = f_{in,AGN} + f_{in,GAL} \quad (5)$$

$$f_{out} = f_{out,AGN} + f_{out,GAL} \quad (6)$$

The relationship between flux and AB magnitude is defined by  $m \equiv -2.5 \log(f_\nu) - 48.6$ . Combining Equations 2 and 3 and converting to flux results in:

$$f_{in,GAL} = X \cdot f_{out,GAL}^B, \quad (7)$$

with  $X = 10^{-0.4(A+48.6-48.6B-C-DC_z-EC_z^2-FC_z^3)}$ .

Equation 4 is similarly converted from magnitude to flux:

$$f_{in,AGN} = Q \cdot f_{out,AGN}^H, \quad (8)$$

with  $Q = 10^{-0.4(G+48.6-48.6H)}$ .

There are now four equations (Equations 5, 6, 7, and 8) that describe the relationships between inner and outer magnitudes for each of the broad-line AGN and galaxy contributions. The quantities  $f_{in}$ ,  $f_{out}$ , and  $C_z$  are measured, and the coefficients  $A$ ,  $B$ ,  $C$ ,  $D$ ,  $E$ ,  $F$ ,  $G$ , and  $H$  come from our line fits in each filter and redshift bin

(with three example filters and redshift bins shown in Figures 4, 5, and 6). Solving these four equations for  $f_{in,AGN}$  results in:

$$f_{in,AGN} = f_{in} - X[f_{out} - (f_{in,AGN}/Q)^{1/H}]^B \quad (9)$$

(with the constants  $X$  and  $Q$  given in equations 7 and 8). We numerically solve this equation using a bisection root-finding method. After solving for  $f_{in,AGN}$ , the other three unknowns can be computed from Equations 5, 6, and 8. This process is repeated to derive AGN-subtracted host galaxy magnitudes in all five bands in each of the ten redshift bins. Table 1 shows the corrected magnitudes and derived stellar masses for the 820 broad-line AGNs in the luminous and faint samples.

### 3.4. Error Analysis

It is necessary to ensure that our AGN/host decomposition method does not introduce errors which bias the resultant host galaxy colors and stellar masses. One assumption of our method is that galaxies have  $\delta m = 0$ : Figure 6 demonstrates that this is true on average, but the  $\delta m$  values of individual galaxies scatter about this value. Similarly the true inner and outer magnitudes of AGN-subtracted host galaxies may have nonzero values of  $\delta m$ , and our correction to  $\delta m = 0$  may introduce systematic errors in their resultant colors and masses.

We investigate the errors of the  $\delta m = 0$  assumption by applying the decomposition method to inactive galaxies. Figure 10 shows the changes in  $(u - z)'$  color and  $M_*$  introduced by “correcting” inactive galaxies to  $\delta m = 0$ . The dispersions in these shifts represent the errors in color and mass from correcting AGN host galaxies with nonzero  $\delta m$ . Errors in color are small because  $\delta u$  and  $\delta z$  are correlated (see Figure 8). The dispersion in stellar mass is slightly larger, as indicated by the error bar in the bottom right of each panel, but mass shifts and dispersions are small among blue cloud and green valley galaxies (the typical hosts of broad-line AGNs). From Figure 10, we do not expect the  $\delta m = 0$  assumption to bias the observed colors and masses of broad-line AGNs.

If our other assumption is incorrect and AGNs contaminate *z*-band concentration, this could also introduce significant errors in the AGN/host decomposition method. Figure 7 shows that the most luminous AGNs ( $M'_{u,AGN} < -20$ ) may bias  $C_z$ , and such systems may have larger systematic or random errors than those estimated in Figure 10. For this reason we eliminate the most luminous AGNs from the discussion and conclusions below. However the low and moderate luminosity broad-line AGNs that make up the bulk of our sample do not exhibit biased  $C_z$ . For these objects the assumption that AGNs do not affect *z*-band concentration is unlikely to cause errors in the AGN/host decomposition.

## 4. THE HOST GALAXIES OF BROAD-LINE AGNS

The corrected galaxy-only photometry of the broad-line AGNs can be used to determine if certain types of host galaxies are more likely to exhibit broad-line AGNs. After computing the AGN-subtracted photometry, we K-correct to  $z = 0.05$  and infer the host galaxy stellar mass using Figure 3. Figure 11 shows total  $(u - z)'$  color vs. luminosity and stellar mass for broad-line AGNs in the

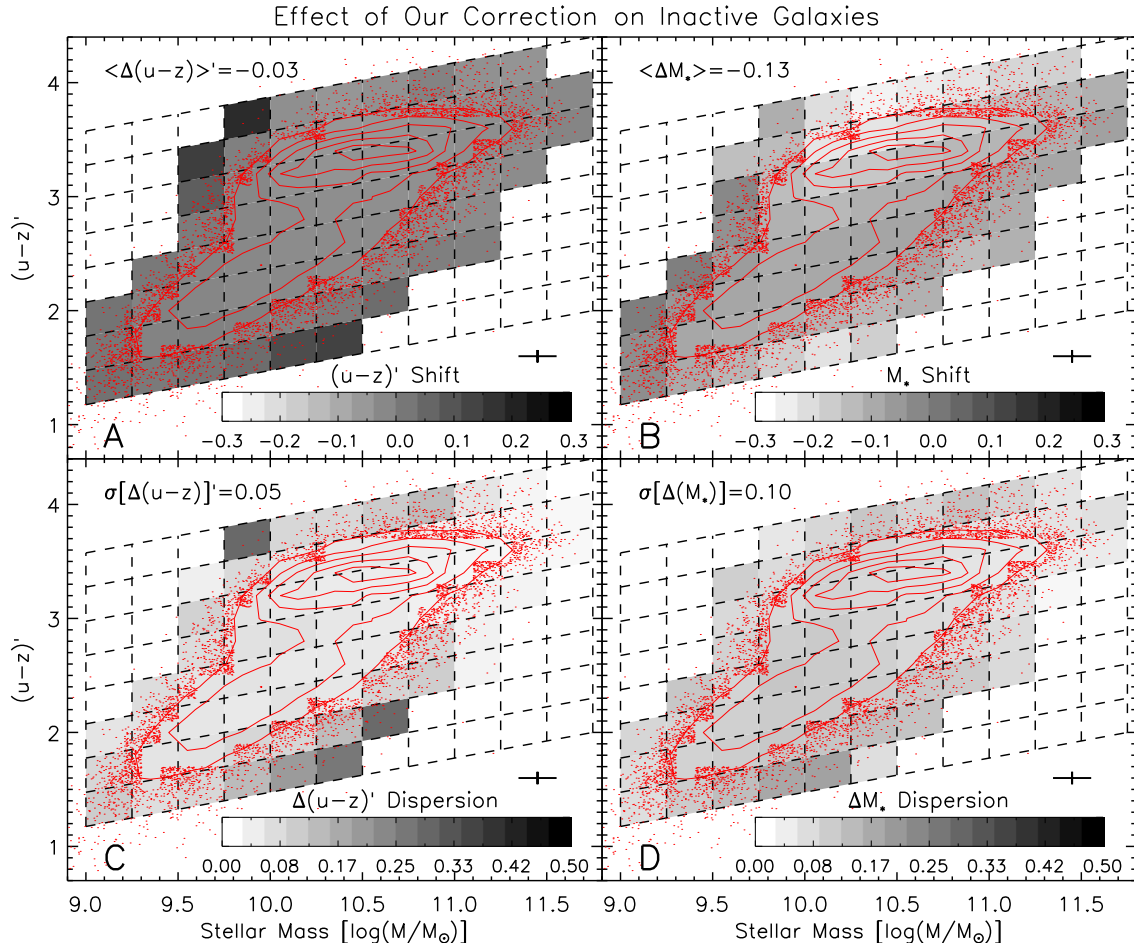


FIG. 10.— Bins in color and stellar mass showing the effects of our AGN/host decomposition method applied to inactive galaxies. The top panels (A and B) show the average shifts in  $(u-z)'$  color and stellar mass, and the bottom panels (C and D) show the dispersion of the changes in color and mass. The text in the upper left of each panel also gives the mean shift or dispersion over all galaxies. Outside of bins with small numbers of galaxies, there are no regions of color-mass space with unusually large shifts or dispersions in corrected color and mass.

faint sample, with contours showing the inactive galaxies for comparison. Figure 12 similarly shows broad-line AGNs and inactive galaxies in the luminous sample.

The top panels of each figure show that broad-line AGNs typically become redder, dimmer, and less massive after recovering the uncontaminated galaxy light. A few AGN hosts become so much redder without the blue point-source AGN that their masses increase, due to the higher mass-to-light ratios of similarly red inactive galaxies. Because we independently correct each filter, there are also a few AGN hosts that become bluer, presumably because they contain a reddened AGN.

To determine if broad-line AGNs are more likely to occur in certain types of galaxies, we measure the fraction of galaxies containing an AGN in bins across the color-mass diagram, as shown in the bottom panels of Figures 11 and 12. Bins are tilted (with slopes of  $\Delta(u-z)'/\Delta M_* = -0.07$  and  $\Delta(u-z)'/\Delta[\log(M_*/M_{\odot})] = 0.3$ ) to be parallel to the red sequence. We count the number of broad-line AGNs with corrected galaxy-only photometry in each bin, then divide by the total number of galaxies (inactive plus active) in that bin to determine the AGN fraction. Table 2 gives the broad-line AGN fraction in each bin of color and mass, as well as the

AGN fraction over the entire mass slice.

In both samples, galaxies on the red sequence are least likely to host a broad-line AGN. Instead AGNs are most likely to be in the bluest host galaxies of a given stellar mass. We further explore what the preference for star-forming hosts means for the AGN-SF connection and AGN feedback in Section 5, but first test to ensure that our results are not caused by selection effects.

#### 4.1. Selection Effects

While broad-line AGNs are the brightest and most rapidly accreting AGNs (e.g., Kollmeier et al. 2006; Trump et al. 2009), many of the weakest broad-line AGNs have significant galaxy contribution to their continua. Dim AGNs could be more difficult to detect in bright galaxies, with the broad lines diluted by host galaxy starlight. More distant galaxies also contain more starlight within the  $3''$  spectroscopic fiber aperture and could similarly dilute the broad emission lines of AGNs.

We test the potential selection bias against dim AGNs in luminous host galaxies by computing the AGN fraction across the color-mass diagram for dim, moderate, and luminous AGNs, as shown in Figure 13. AGN strength is quantified using the AGN-only  $u$ -band absolute mag-

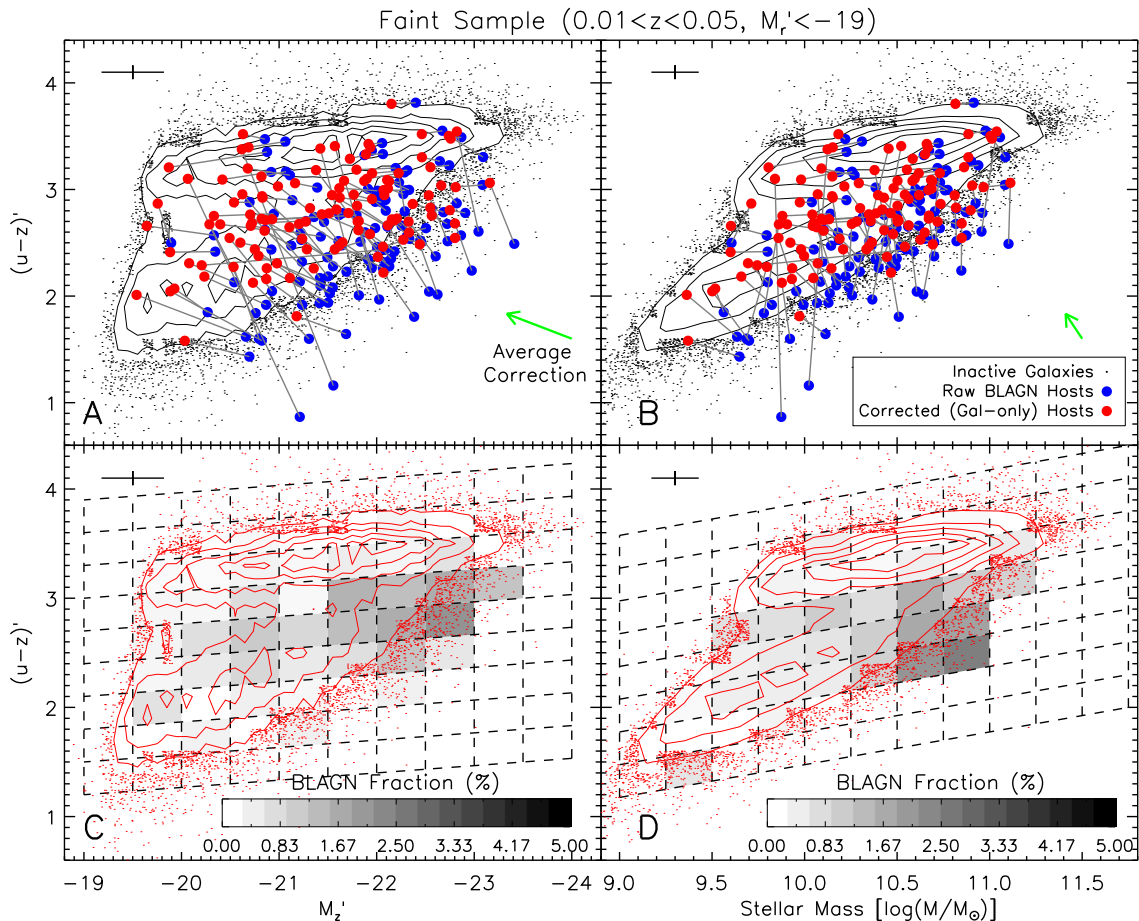


FIG. 11.— The color-luminosity and color-mass diagrams for inactive galaxies and broad-line AGN hosts in the faint sample ( $M_r' < -19$  and  $0.01 < z < 0.05$ ). The top panels (A and B) shows total  $(u-z)'$  color vs. luminosity and stellar mass for both uncorrected broad-line AGNs (blue filled circles) and AGN-subtracted host galaxies (red filled circles), with lines connecting the two measurements of each AGN. The mean AGN subtraction vectors are shown by the green arrows. The bottom panels (C and D) show the broad-line AGN frequency in bins of color and luminosity or color and mass, using the corrected AGN host properties. The typical scatter of our AGN/host decomposition method (see Section 3.4) is shown by error bars in the upper left of each panel, and contours and points represent the inactive galaxy populations. Star-forming (blue cloud and green valley) galaxies are the most common hosts of broad-line AGNs.

nitude, with  $M_{u, \text{AGN}}$  divisions chosen to put the same number of AGNs in each set. AGNs were drawn from the faint sample because it includes a large range in stellar mass. From Figure 13 it is clear that dim AGNs are not found less frequently in massive, luminous galaxies, and so this potential selection effect does not occur in our sample.

Figure 14 similarly tests the potential selection effect of higher distance biasing against AGN identification. The luminous sample is most appropriate for this test because it includes luminosity-limited AGNs over the full redshift range  $0.01 < z < 0.11$ . In addition to measuring the broad-line AGN fraction over all galaxies in each redshift bin, a set of “massive” galaxies is also defined with  $\log(M_*/M_\odot) > 9.5 + 0.5(u-z)'$ . This mass limit corresponds to the most massive 10% of galaxies along the blue cloud and green valley.

Over the limited  $0.01 < z < 0.11$  redshift range of our sample, there is no evidence for a decline in the fraction of galaxies hosting a broad-line AGN at higher distance. For this reason we do not expect distant galaxies to bias against AGN identification through starlight dilution in the spectroscopic aperture.

## 5. DISCUSSION

In this section we discuss the consequences of AGN hosts with young stellar populations for the coevolving growth of galaxies and supermassive black holes.

### 5.1. AGNs and Star Formation

A major finding of this study is that broad-line AGNs tend to lie in hosts with young stellar populations, and avoid red and quiescent host galaxies. The simplest explanation for this is if the same gas that fuels rapidly accreting, unobscured nuclear activity also rapidly formed stars in the recent past. Figure 13 suggests that the more powerful the broad-line AGN, the bluer the host galaxy: more rapidly accreting AGNs may have more powerful recent star formation in their host galaxy. Once again, this suggests that star formation and nuclear activity are fueled by the same material.

Figure 15 directly compares the broad-line AGN luminosity to the color and stellar mass of the host galaxy. AGN luminosity is quantified by AGN-only  $M_{u, \text{AGN}}'$ . In addition to corrected color and mass for broad-line AGN hosts, Figure 15 also shows the offsets in each of these quantities from inactive galaxies of similar (within



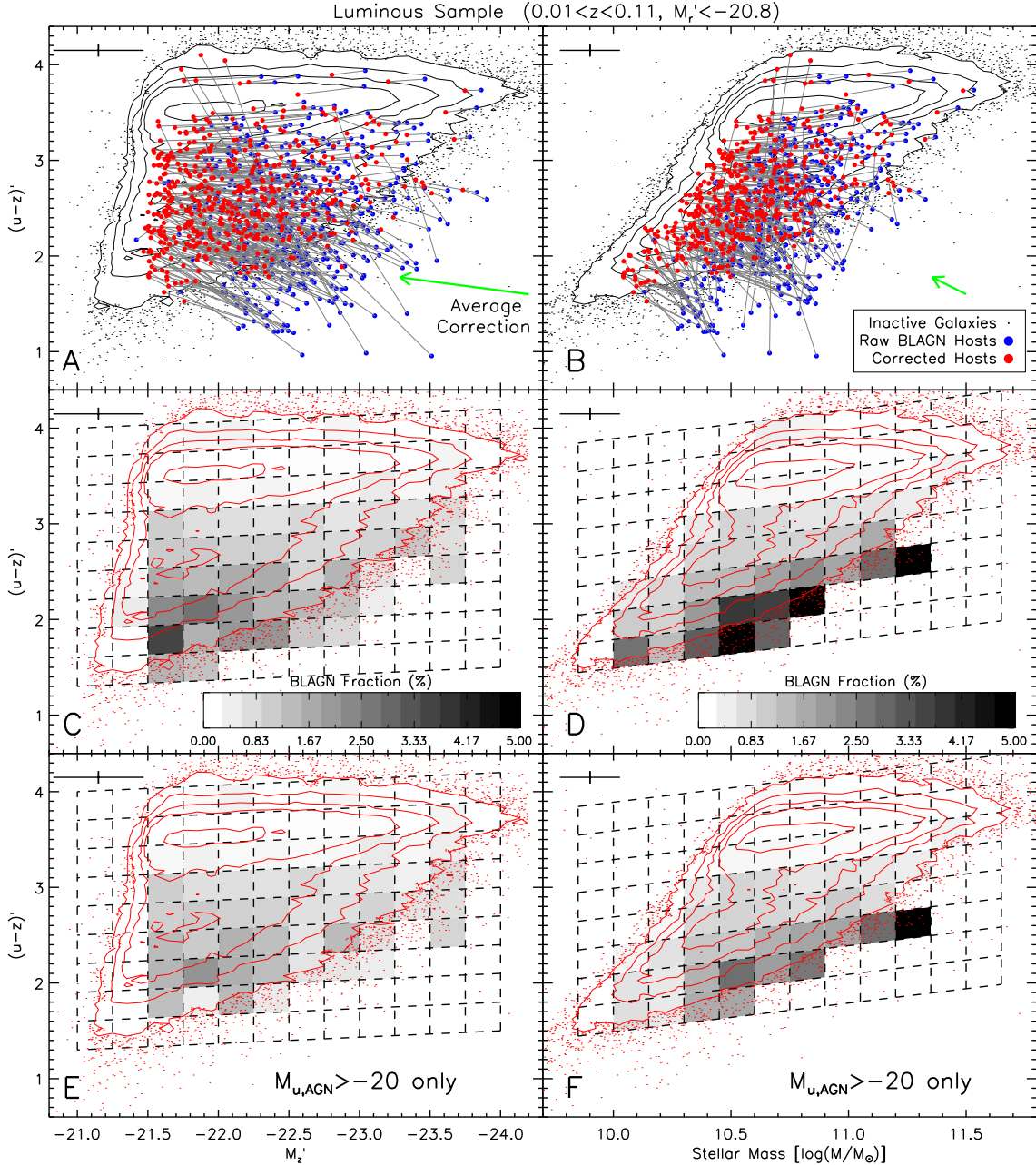


FIG. 12.— The color-luminosity and color-mass diagrams for inactive galaxies and broad-line AGN hosts in the luminous sample ( $M_r' < -20.8$  and  $0.01 < z < 0.11$ ). The top panels (A and B) show uncorrected (blue) and corrected (red) total  $(u-z)'$  color vs. luminosity and stellar mass for broad-line AGN hosts, and the middle panels (C and D) show the AGN frequency in bins of color and luminosity or color and mass. The bottom panels (E and F) include only AGN hosts with  $M_{u,AGN}' > -20$ : that is, AGNs with potentially biased  $C_z$  are removed. Error bars in the upper left of each panel represent the typical scatter introduced by AGN/host decomposition (see Section 3.4), and inactive galaxies are shown by contours and points. As in the faint sample, broad-line AGNs are most common in the bluest galaxies

of a given stellar mass. These offsets are useful to remove the degeneracy between a galaxy's mass and its color. For example, the apparent anti-correlation between stellar mass and AGN luminosity in Panel C is a result of the degeneracy between mass and color. Comparing AGNs and inactive galaxies of similar color, Panel D shows no significant trend between stellar mass offset and AGN luminosity.

Panel B in Figure 15 shows that more luminous AGNs have bluer host galaxies in both the luminous and faint

samples. This may represent a physical connection between AGN luminosity and the host galaxy's recent star formation history. AGN luminosity probably translates to accretion rate, and so the relationship between AGN  $M_{u,AGN}'$  and host color indicates that AGN accretion rate is correlated with the number of recently formed stars. These observations favor scenarios with similar fuel sources for both star formation and nuclear activity (e.g., Salim et al. 2007; Silverman et al. 2009), with little or no time delay between the processes fueling each.

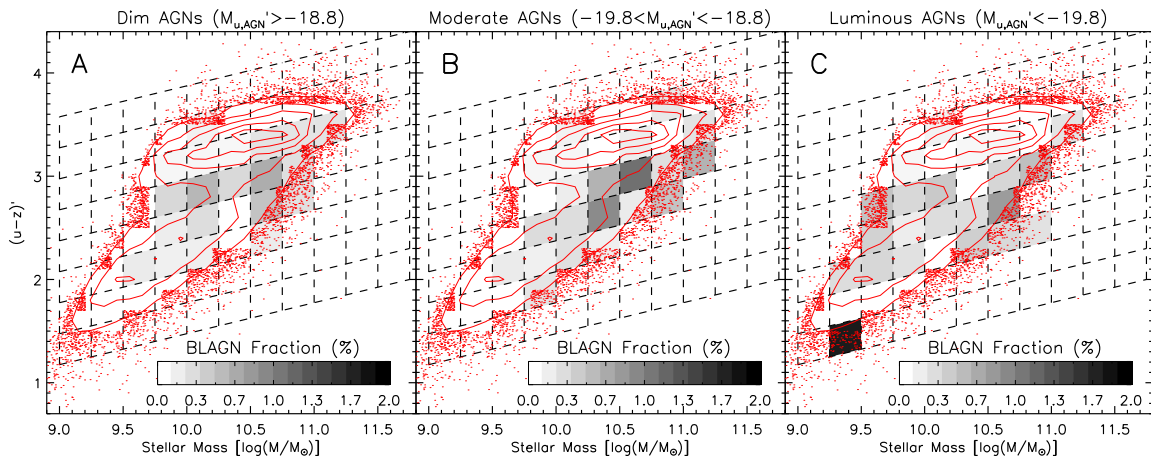


FIG. 13.— The frequency of dim ( $M'_{u,AGN} > -18.8$ ), moderate ( $-19.8 < M'_{u,AGN} < -18.8$ ), and luminous ( $M'_{u,AGN} < -19.8$ ) broad-line AGNs across the color-mass diagram, drawn from the faint sample ( $M'_r < -19$ ,  $0.01 < z < 0.05$ ). The red contours and points show the inactive galaxy population. As in Figures 11 and 12, the AGN fraction is calculated in each bin using the corrected galaxy-only photometry. Dim AGNs are no less likely to be in high-mass galaxies than strong AGNs, suggesting that there are no selection effects against identifying dim AGNs in bright galaxies.

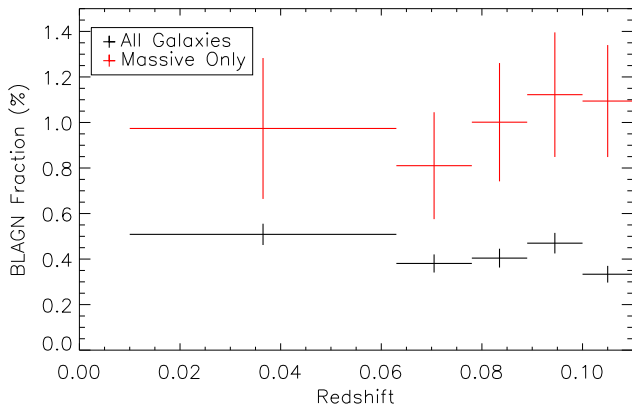


FIG. 14.— The fraction of galaxies from the luminous sample containing a broad-line AGN with redshift. Black lines show the population of all galaxies, while red lines show only with  $\log(M_*/M_\odot) > 9.5 + 0.5(u - z)'$  (this corresponds to the most massive 10% of galaxies on the blue cloud and green valley). Each redshift bin contains the same number of inactive galaxies, and the vertical error bars indicate the  $1\sigma$  error assuming Poissonian statistics. There is no evidence for fewer broad-line AGNs at higher redshift, suggesting that our sample is quite complete.

This interpretation is robust even given the limitations of our AGN/galaxy decomposition method. Recall the assumption that AGN host galaxies have the same light distributions as inactive galaxies (quantified by  $\delta m = 0$ ). Given the  $M - \sigma$  relation (e.g. Park et al. 2012) and requirement of a bulge to host an AGN, it is unlikely that broad-line AGNs have hosts with intrinsic  $\delta m < 0$ . On the other hand, the unusual blue colors of broad-line AGN hosts might indicate nuclear starbursts and intrinsic  $\delta u > 0$ . Applying our decomposition method to an AGN host with a nuclear starburst would over-subtract the blue light, resulting in a redder corrected galaxy  $(u - z)'$  color. With the presence of a nuclear starburst it is possible that the galaxy colors of AGN hosts may be even bluer than we observe. Similarly the connection between AGN luminosity and blue host color in Figure 15 would steepen if these blue hosts contain

nuclear starbursts and unusually concentrated blue light.

Another potential concern is that the broad-line AGN host galaxies appear blue due to extended scattered light from the AGN. Zakamska et al. (2006) noted that in extreme cases Type 2 quasars with  $M_{B,AGN} < -24$  have scattered light on  $>1$  kpc scales that dominates over the host galaxy starlight. Measuring extended scattered light for our sample is beyond the scope of this work, given the requirement for long-slit spectropolarimetry on a large number of broad-line AGNs with varying luminosities. However we note that our broad-line AGNs are several (4-7) magnitudes fainter than the Zakamska et al. (2006) sample, and so we assume the amount of extended scattered light in this work to be negligible.

## 5.2. The Different Hosts of Luminous Broad-Line and Weak Narrow-Line AGNs

Our large sample of broad-line AGNs from the SDSS shows a strong preference for blue host galaxies. This matches earlier studies with small broad-line AGN samples, which found a similar preference for hosts with young stellar populations (Bahcall et al. 1997; Jahnke et al. 2004a,b). The most [OIII]-luminous narrow-line AGNs also prefer star-forming host galaxies (Kauffmann et al. 2003b; Silverman et al. 2009). These classes of luminous AGNs all represent “feast mode” rapid accretion with high Eddington ratios ( $\lambda_{Edd}$ ): Kauffmann & Heckman (2009) estimate that the most [OIII]-luminous narrow-line AGNs have  $\lambda_{Edd} \sim 0.1$ , and broad-line AGNs also have Eddington ratios of 1-100% (Kollmeier et al. 2006; Trump et al. 2009). In future work we will directly measure and compare  $\lambda_{Edd}$  in our broad-line AGN sample, but for now we simply assume that they are rapidly accreting AGNs with  $\lambda_{Edd} > 0.01$ .

The blue hosts of our broad-line AGNs are in contrast to the hosts of fainter narrow-line AGNs, which instead prefer green valley galaxies (Nandra et al. 2007; Salim et al. 2007; Georgakakis et al. 2008; Silverman et al. 2008; Gabor et al. 2009; Schawinski et al. 2009; Hickox et al. 2009; Kocevski et al. 2009) or all galaxy types equally

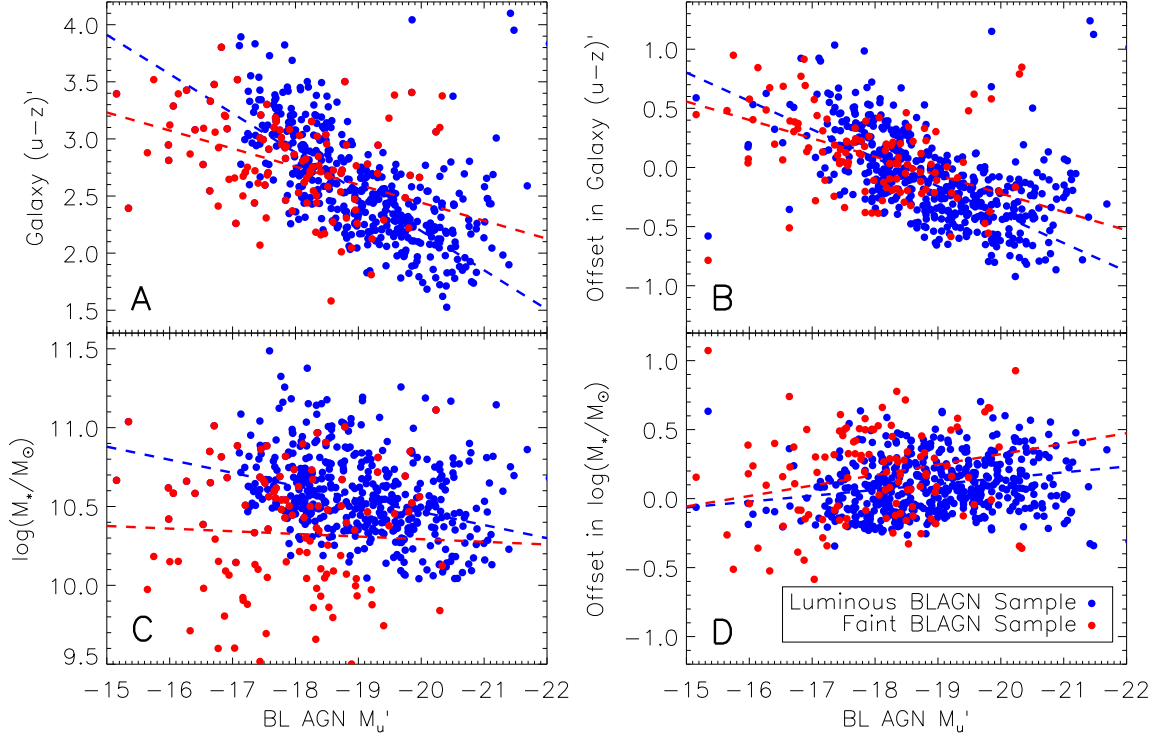


FIG. 15.— Corrected host galaxy  $(u-z)'$  color and stellar mass vs. AGN luminosity  $M'_{u}$ . Panel B (top right) shows the color offsets of broad-line AGNs, defined as the difference between the corrected AGN host color and the median color of inactive galaxies with similar mass. Similarly Panel D (bottom right) shows the offset in BL AGN host stellar mass from the median stellar mass of inactive galaxies with similar color. Red points show the faint broad-line AGN sample ( $M'_{u} < -19$ ,  $0.01 < z < 0.05$ ), while blue points show the luminous sample ( $M'_{u} < -20.8$ ,  $0.01 < z < 0.11$ ). Dashed lines indicate the best-fit line for AGNs with  $M'_{u,AGN} > -20$ : the fit excludes the most luminous AGNs because they may have biased  $C_z$  measurements (see Section 3.1 and Figure 7). Galaxies hosting more powerful AGNs typically have younger stellar populations, suggesting that the same gas needed to fuel a broad-line AGN also drives recent star formation activity.

(Xue et al. 2010). The host-dominated AGNs of these previous studies are, by construction, fainter than broad-line AGNs, due to either obscuration or lower accretion rates ( $\lambda_{Edd} < 0.01$ ). Different host galaxies for broad-line AGNs and weaker host-dominated AGNs are incompatible with the historical AGN unified model (Antonucci et al. 1993). In its simplest version, the unified model uses only geometrical orientation to explain the different observed properties of broad-line and host-dominated AGNs. Both broad-line and host-dominated AGNs would then be observed in the same host galaxy types, as has been observed among intermediate-luminosity AGNs at  $z \sim 1$  (Ammons et al. 2011). Our observations instead favor AGN unified models where broad-line and faint narrow-line AGNs have physically different accretion properties (Ho 2008; Trump et al. 2011; Antonucci et al. 2011). Broad-line AGNs might be in star-forming galaxies because such galaxies have the most abundant or efficient fuel supply for the SMBH, while other galaxy types can fuel only “famine-mode” host-dominated AGNs with low accretion rates (Kauffmann & Heckman 2009; Schawinski et al. 2010).

Kauffmann et al. (2003b) used a large sample of host-dominated AGNs to show that there may be a minimum stellar mass of  $\log(M_*/M_\odot) > 10.5$  required for a galaxy to host an AGN. Recently, however, Aird et al. (2012) argued that the apparent preference for massive AGN

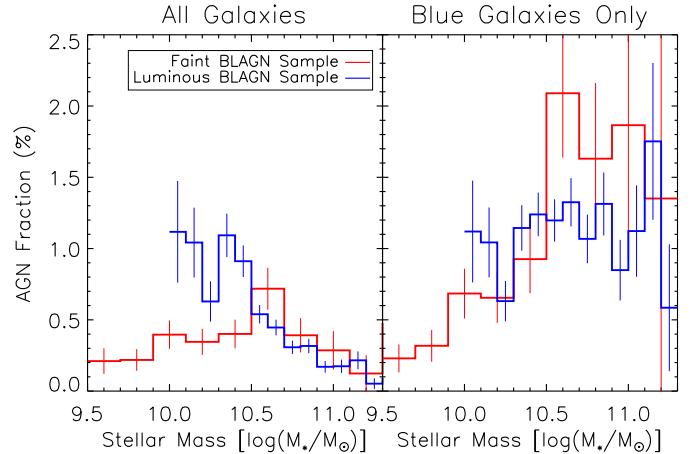


FIG. 16.— The percentage of AGNs found in hosts of varied stellar masses, for both the faint (red lines) and luminous (blue lines) broad-line AGN samples. Vertical lines give the Poissonian errors in each bin. At left, the luminous sample suggests that AGNs are more common in low-mass galaxies, but this is driven purely by the preference for blue hosts. The right panel instead shows the AGN fraction in blue galaxies with  $(u-z)' < 0.3 \log(M_*/M_\odot)$ . Here AGNs in the luminous sample have equivalent likelihoods to be in hosts of any stellar mass, in agreement with Aird et al. (2012). Meanwhile, the faint sample may show a preference for AGNs in high-mass hosts, but this is not significant and is perhaps the result of small number statistics or incompleteness at  $\log(M_*/M_\odot) < 10$ .

hosts is caused by selection effects, and there is instead a universal Eddington-ratio distribution of AGNs in galaxies of any stellar mass. Figure 16 shows the percentage of broad-line AGNs with host stellar mass for both the luminous and faint samples. Given the narrow distribution of high Eddington ratios for broad-line AGNs ( $0.01 < L/L_{Edd} < 1$ , e.g., Kollmeier et al. 2006; Trump et al. 2009), our AGN sample is complete to  $\log(M_*/M_\odot) \sim 10$  (Kelly & Shen 2012). Thus the luminous broad-line AGN sample (also limited by  $\log(M_*/M_\odot) > 10$ ) provides a direct test of the AGN dependence on host stellar mass. After controlling for galaxy color (right panel of Figure 16), we find a flat AGN fraction with stellar mass. This suggests that there is no stellar mass threshold for broad-line AGNs, in agreement with Aird et al. (2012).

### 5.3. Consequences for AGN Feedback

Theoretical simulations invoke feedback from luminous AGNs to rapidly quench star formation and transform their host galaxy colors from blue to red (Silk & Rees 1998; Fabian 2002; Di Matteo, Springel, & Hernquist 2005). Several authors have claimed observational evidence for this scenario, with host-dominated AGNs apparently preferring recently-quenched green valley galaxies (Nandra et al. 2007; Georgakakis et al. 2008; Schawinski et al. 2009; Hickox et al. 2009; Kocevski et al. 2009). Since radiative-mode feedback scales with AGN strength, the broad-line AGNs in our sample would be expected to have an even greater effect in quenching star formation. However, we find precisely the opposite effect: more powerful AGNs seem to lie in bluer galaxies. If quasar winds cause significant feedback, then their galaxy-wide effects are not visible until after the broad-line AGN disappears.

Figure 17 outlines three scenarios connecting AGNs and galaxy quenching: scenario A has star formation quenched before the broad-line AGN phase, scenario B quenches during the broad-line AGN peak, and scenario C has star formation quenched well after the broad-line AGN phase. The increase in star formation during the AGN peak in all scenarios is motivated by our observed connection between AGN luminosity and blue host galaxy color. The broad-line AGN phase occurs only during the most luminous AGN activity, which means

that our study probes only the region limited by the dashed “BL AGN Visible” lines in each panel.

Scenario A is immediately ruled out by the observed absence of broad-line AGNs among quenched red galaxies. However our observations cannot distinguish between quenching during or after the broad-line AGN phase (scenarios B and C). The broad-line AGN lifetime is less than  $\sim 100$  Myr (Martini 2004), which is roughly the same amount of time it takes for galaxy colors to change from blue to green or red after star formation quenches (e.g., Bruzual & Charlot 2003). Even if quenching occurs during the AGN peak, a change in galaxy colors would not be observed until after the broad-line AGN fades. This is evident in the scenario B curve in the right panel of Figure 17. So while our observations exclude AGN quenching scenarios that occur before the broad-line AGN phase, only observations of fading AGNs can distinguish between simultaneous or delayed AGN quenching.

## 6. SUMMARY

An aperture photometry method is used to disentangle the light of broad-line AGNs and their host galaxies at  $0.01 < z < 0.11$ . Based on the corrected, host-only photometry, broad-line AGNs are distributed throughout the blue cloud and green valley but are very rare among red sequence hosts. Within this distribution, AGN strength is correlated to the youth of the host galaxy stellar population, such that bluer galaxies have more luminous broad-line AGNs. This suggests that broad-line AGN activity and star formation are closely coeval with little or no delay between the ignition of each. The host galaxy properties of broad-line AGN hosts also suggest that quenching of galactic star formation occurs or becomes visible only after the rapidly accreting SMBH phase: quasar winds are either unconnected to quenching, or their effects are apparent only after the broad-line AGN phase has ended.

The authors from UCSC acknowledge support from NASA HST grant GO 12060.10-A, Chandra grant G08-9129A, and NSF grant AST- 0808133. Helpful discussions with Edmond Cheung and Hassen Yesuf contributed to the development of this work. AH acknowledges support from the UC Santa Cruz Science Internship Program.

## REFERENCES

- Aird, J. et al. 2012, ApJ, 746, 90  
 Ammons, S. M. et al. 2011, ApJ, 740, 3  
 Antonucci, R. 1993, ARA&A, 31, 473  
 Antonucci, R. 2011, arXiv:1101.0837  
 Bahcall, J. N., Kirhakos, S., Saxe, D. H. & Schneider, D. P. 1997, ApJ, 479, 642  
 Baldwin, J. A., Phillips, M. M. & Terlevich, R. 1981, PASP, 93, 5  
 Bell, E. F. et al. 2011, ApJ submitted (arXiv:1110.3786)  
 Blanton, M. R. & Roweis, S. 2007, AJ, 133, 734  
 Brinchmann, J. & Ellis, R. S. 2000, ApJL, 536, 77  
 Bruzual, G. & Charlot, S. 2003, MNRAS, 344, 1000  
 Cardamone, C. N., Urry, C. M., Schawinski, K., Treister, E., Brammer, G. & Gawiser, E. 2010, ApJ, 721, 38  
 Cheung, E. et al. 2012, in prep.  
 Cisternas, M. et al. 2011, ApJ, 726, 57  
 Croton, D. J. et al. 2006, MNRAS, 365, 11  
 Di Matteo, T., Springel, V., & Hernquist, L. 2005, Nature, 433, 604  
 Driver, S. P. et al. 2006, MNRAS, 368, 414  
 Fabian, A. C. 2002, MNRAS, 308, 39  
 Ferrarese, L. & Merritt, D. 2000, ApJ, 593, 9  
 Gabor, J. M. et al. 2009, ApJ, 691, 705  
 Ganguly, R. & Brotherton, M. S. 2008, 672, 102  
 Gebhardt, K. et al. 2000, ApJ, 539, 13  
 Georgakakis, A. et al. 2008, MNRAS, 385, 2049  
 Haggard, D., Green, P. J., Anderson, S. F., Constantin, A., Aldcroft, T. L., Kim, D.-W. & Barkhouse, W. A. 2010, ApJ, 723, 1447  
 Heckman, T. M. & Kauffmann, G. 2006, NewAR, 50, 677  
 Hickox, R. C. et al. 2009, ApJ, 696, 891  
 Ho, L. C. 2008, ARA&A, 46, 475  
 Hopkins, P. F., Hernquist, L., Cox, T. J., DiMatteo, T., Robertson, B. & Springel, V. 2008, ApJS, 175, 356  
 Hopkins, P. F., Hernquist, L., Cox, T. J. & Keres, D. 2008, ApJS, 175, 356

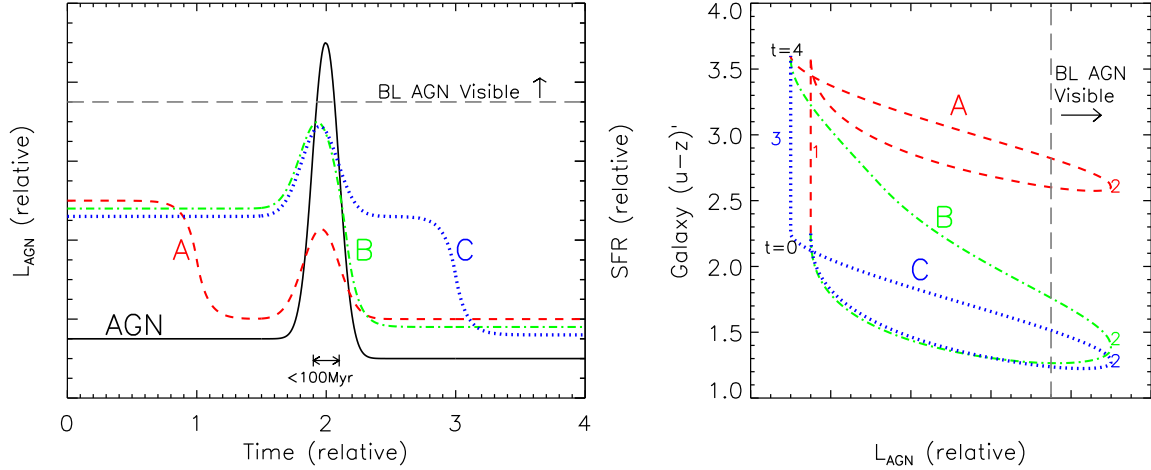


FIG. 17.— A phenomenological model outlining three scenarios connecting AGN activity and the quenching of star formation. The broad-line AGN phase is parameterized as a Gaussian function with a width of less than 100 Myr (Martini 2004), and the three curves A, B, and C represent star formation rates with quenching occurring before, during, and after the broad-line AGN phase. The left panel shows the evolution of the AGN and SFR functions with time, and the right panel shows the expected galaxy colors vs. AGN luminosity for the same curves. Numerals along the curves in the right panel correspond to times from the left panel ( $t = 1$  is not shown for curves B or C because it is identical to  $t = 0$ , just as  $t = 3$  is the same as  $t = 4$  for curves A and B). Our observations rule out scenario A, but allow for quenching either during or after the broad-line AGN phase as shown by curves B and C.

Jahnke, K., Kuhlbrodt, B. & Wisotzki, L. 2004a, MNRAS, 352, 399  
 Jahnke, K. et al. 2004b, ApJ, 614, 568  
 Kauffmann, G. et al. 2003a, MNRAS, 341, 33  
 Kauffmann, G. et al. 2003b, MNRAS, 346, 1055  
 Kauffmann, G. & Heckman, T. M. 2009, MNRAS, 397, 135  
 Kelly, B. C. & Shen, Y. 2012, ApJ submitted (arXiv:1209.0477)  
 Kewley, L. J., Groves, B., Kauffmann, G. & Heckman, T. 2006, MNRAS, 372, 961  
 Kocevski, D. D., Lubin, L. M., Lemaux, B. C., Gal, R. R., Fassnacht, C. D., Lin, R. & Squires, G. K. 2009, ApJ, 700, 901  
 Kocevski, D. D. et al. 2012, ApJ, 744, 148  
 Kollmeier, J. A. et al. 2006, ApJ, 648, 128  
 Magorrian, J. et al. 1998, AJ, 115, 2285  
 Marconi, A. & Hunt, L. K. 2003, ApJ, 589, 21  
 Martini, P. 2004, Carnegie Observatories Astrophysics Series, Vol 1: Coevolution of Black Holes and Galaxies, ed. L. C. Ho (Cambridge: Cambridge Univ. Press), 170  
 Mullaney, J. R. et al. 2012, MNRAS, 419, 95  
 Nandra, K. Georgakakis, A., Willmer, C. N. A., Cooper, M. C., Croton, D. J., Davis, M., Faber, S. M., Koo, D. C., Laird, E. S. & Newman, J. A. 2007, ApJ, 660, 11  
 Park, D., Kelly, B. C., Woo, J.-H. & Treu, T. 2012, ApJ in press (arXiv:1209.3773)  
 Peng, C. Y., Ho, L. C., Impey, C. D. & Rix H.-W. 2002, AJ, 124, 266  
 Richards, G. T. et al. 2002, AJ, 123, 2945  
 Rigby, J. R., Rieke, G. H., Donley, J. L., Alonso-Hererro, A. & Perez-Gonzalez, P. G. 2006, ApJ, 645, 115  
 Rovilos, E. et al. 2012, A&A in press (arXiv:1207.7129)  
 Salim, S. et al. 2007, ApJS, 173, 267  
 Santini, P et al. 2012, A&A, 540, 109  
 Schawinski, K., Virani, S., Simmons, B., Urry, C. M., Treister, E., Kaviraj, S. & Kushkuley, B. 2009, ApJ, 692, 19  
 Schawinski, K. et al. 2010, ApJ, 711, 284  
 Sérsic, J. L. 1968, Atlas de Galaxias Australes (Cordoba: Obbs. Astron. Univ. Nacional Cordoba)  
 Silk, J. & Rees, M. J. 1998, A&A, 331, 1  
 Silverman, J. D. et al. 2008, ApJ, 675, 1025  
 Silverman, J. D. et al. 2009, ApJ, 696, 396  
 Strauss, M. A. et al. 2002, AJ, 124, 1810  
 Trump, J. R. et al. 2009, ApJ, 700, 49  
 Trump, J. R. et al. 2011, ApJ, 733, 60  
 Vanden Berk, D. E. et al. 2001, AJ, 122, 549  
 Winter, L. M. 2010, ApJ, 725, 126  
 Wuyts, S. et al. 2011, ApJ, 742, 96  
 Xue, Y. Q., Brandt, W. N., Luo, B., Rafferty, D. A., Alexander, D. M., Bauer, F. E., Lehmer, B. D., Schneider, D. P. & Silverman, J. D. 2010, ApJ, 720, 368  
 Yesuf, H., Faber, S. M., Trump, J. R., Koo, D. C. & Fang, J. J. 2012, in prep.  
 York, D. G. et al. 2000, AJ, 120, 1579  
 Zakamska, N. L., Strauss, M. A., Krolik, J. H., Ridgway, S. E., Schmidt, G. D., Smith, P. S., Heckman, T. M., Schneider, D. P., Hao, L. & Brinkmann, J. 2006, AJ, 132, 1496

TABLE 1  
 RAW AND CORRECTED MEASUREMENTS OF BROAD-LINE AGN HOSTS <sup>a</sup>

SDSS ID	RA	Dec	redshift	$M_z^b$	Raw $u^b$	Cor. $u^b$	$\delta u$	$C_z$	$(u-z)^b$	$\log(M_*/M_\odot)$
587732484349100048	147.638145	44.314366	0.0153	-20.21	16.73	17.00	0.40	4.19	3.52	10.18
587742060556648547	233.968767	14.517718	0.0195	-20.66	15.94	16.18	1.16	2.25	2.65	10.06
587735240099954710	129.386277	28.705193	0.0114	-21.35	14.88	14.92	0.21	2.20	3.39	10.67
587734948589273110	146.372371	9.602890	0.0133	-19.46	16.41	16.91	1.02	2.86	2.87	9.71
587739811560882185	214.498122	25.136867	0.0165	-21.81	14.78	15.20	1.70	3.09	3.15	10.73
587724242842026028	52.555273	-5.543318	0.0131	-20.91	14.91	14.99	0.35	2.55	2.81	10.42
587734622701093005	121.411097	26.168188	0.0170	-21.52	15.15	15.21	0.63	1.90	2.95	10.62
587735695380578421	224.278321	49.669022	0.0134	-20.93	14.57	14.72	0.99	2.85	2.26	10.15
587725039018311737	180.309815	-3.678079	0.0196	-20.46	15.46	16.39	2.23	2.74	2.27	9.80
587738946662629527	129.545598	24.895276	0.0284	-21.76	16.09	16.31	0.70	2.71	3.30	10.89
587732577773420642	161.215528	6.596847	0.0276	-22.37	15.11	15.15	0.03	2.09	2.55	10.85

TABLE 1 — *Continued*

SDSS ID	RA	Dec	redshift	$M_z^b$	Raw $u^b$	Cor. $u^b$	$\delta u$	$C_z$	$(u - z)^b$	$\log(M_*/M_\odot)$
587738616483282976	154.956204	33.367703	0.0232	-19.77	16.10	17.41	2.16	3.00	2.67	9.86
587726014003216406	198.274215	1.465540	0.0294	-20.22	17.31	17.64	0.32	2.78	2.92	10.15
587733080809668634	171.400663	54.382551	0.0206	-19.18	17.00	17.78	1.19	3.03	2.66	9.60
587741490361204744	141.827109	23.020102	0.0263	-21.76	16.18	16.36	0.27	3.00	3.52	10.89
587732771575955522	144.551130	7.727765	0.0219	-20.08	16.92	17.42	0.83	3.01	3.20	10.09
587729233053417523	251.839456	44.702715	0.0254	-19.98	17.41	17.57	-0.31	2.54	2.88	9.97
587733603730063381	245.053147	40.151711	0.0285	-20.42	16.16	16.77	1.43	3.11	2.16	9.93
588010359086579732	180.740878	4.845853	0.0207	-21.37	15.87	15.98	0.96	1.89	3.08	10.58

<sup>a</sup> The full catalog of 820 broad-line AGNs appears as a machine-readable table in the electronic version. In addition to the columns shown here, the full catalog includes raw and corrected magnitudes and  $\delta m$  measurements for all five *ugriz* filters.

<sup>b</sup> All magnitudes are K-corrected to  $z = 0.05$  and given in AB units.

TABLE 2  
 BROAD-LINE AGN FRACTIONS WITH HOST GALAXY STELLAR MASS AND  
 COLOR

Lower Left Bin <sup>a</sup>		Faint Sample			Luminous Sample		
$\log(M_*/M_\odot)$	$(u-z)'$	$N_{\text{gal}}$	$N_{\text{AGN}}$	BL AGN %	$N_{\text{gal}}$	$N_{\text{AGN}}$	BL AGN %
9.00	1.175	208	0	0	0	0	0
9.00	1.475	500	0	0	0	0	0
9.00	1.775	123	0	0	0	0	0
9.00	all colors	835	0	0	0	0	0
9.25	1.250	198	1	$0.51 \pm 0.51$	0	0	0
9.25	1.550	835	0	0	0	0	0
9.25	1.850	979	1	$0.10 \pm 0.10$	0	0	0
9.25	2.150	213	0	0	0	0	0
9.25	2.450	18	0	0	0	0	0
9.25	all colors	2246	2	$0.09 \pm 0.06$	0	0	0
9.50	1.325	136	0	0	0	0	0
9.50	1.625	769	0	0	0	0	0
9.50	1.925	1292	4	$0.31 \pm 0.16$	0	0	0
9.50	2.225	711	2	$0.28 \pm 0.20$	0	0	0
9.50	2.525	330	2	$0.61 \pm 0.43$	0	0	0
9.50	2.825	442	0	0	0	0	0
9.50	3.125	50	0	0	0	0	0
9.50	all colors	3731	8	$0.21 \pm 0.08$	0	0	0
9.75	1.400	58	0	0	354	0	0
9.75	1.700	462	1	$0.22 \pm 0.22$	272	0	0
9.75	2.000	1249	4	$0.32 \pm 0.16$	22	0	0
9.75	2.300	997	4	$0.40 \pm 0.20$	1	0	0
9.75	2.600	668	4	$0.60 \pm 0.30$	1	0	0
9.75	2.900	1301	3	$0.23 \pm 0.13$	0	0	0
9.75	3.200	677	0	0	2	0	0
9.75	3.500	31	0	0	2	0	0
9.75	all colors	5443	16	$0.29 \pm 0.07$	654	0	0
10.00	1.475	19	0	0	438	10	$2.28 \pm 0.73$
10.00	1.775	222	0	0	1929	18	$0.93 \pm 0.22$
10.00	2.075	844	3	$0.36 \pm 0.21$	1950	12	$0.62 \pm 0.18$
10.00	2.375	1141	6	$0.53 \pm 0.22$	326	0	0
10.00	2.675	821	8	$0.97 \pm 0.35$	59	0	0
10.00	2.975	1691	2	$0.12 \pm 0.08$	3	0	0
10.00	3.275	974	3	$0.31 \pm 0.18$	2	0	0
10.00	3.575	50	0	0	1	0	0
10.00	all colors	5762	22	$0.38 \pm 0.08$	4708	40	$0.85 \pm 0.13$
10.25	1.550	8	0	0	200	9	$4.50 \pm 1.53$
10.25	1.850	90	0	0	1510	31	$2.05 \pm 0.37$
10.25	2.150	449	4	$0.89 \pm 0.45$	4762	61	$1.28 \pm 0.17$
10.25	2.450	942	9	$0.96 \pm 0.32$	4807	37	$0.77 \pm 0.13$
10.25	2.750	939	6	$0.64 \pm 0.26$	2513	21	$0.84 \pm 0.18$
10.25	3.050	1933	2	$0.10 \pm 0.07$	2291	1	$0.04 \pm 0.04$
10.25	3.350	1211	0	0	493	0	0
10.25	3.650	72	0	0	6	0	0
10.25	all colors	5644	21	$0.37 \pm 0.08$	16582	160	$0.96 \pm 0.08$
10.50	1.625	4	0	0	54	1	$1.85 \pm 1.87$
10.50	1.925	16	0	0	511	21	$4.11 \pm 0.92$
10.50	2.225	142	3	$2.11 \pm 1.23$	2617	44	$1.68 \pm 0.26$
10.50	2.525	530	9	$1.70 \pm 0.57$	5406	49	$0.91 \pm 0.13$
10.50	2.825	834	13	$1.56 \pm 0.44$	5584	40	$0.72 \pm 0.11$
10.50	3.125	1957	6	$0.31 \pm 0.13$	11466	22	$0.19 \pm 0.04$
10.50	3.425	1205	0	0	12747	1	$0.01 \pm 0.01$
10.50	3.725	81	0	0	1220	3	$0.25 \pm 0.14$
10.50	all colors	4769	31	$0.65 \pm 0.12$	39605	181	$0.46 \pm 0.03$
10.75	1.700	0	0	0	16	0	0
10.75	2.000	1	0	0	114	7	$6.14 \pm 2.39$
10.75	2.300	39	1	$2.56 \pm 2.60$	842	21	$2.49 \pm 0.55$
10.75	2.600	163	3	$1.84 \pm 1.07$	2419	21	$0.87 \pm 0.19$
10.75	2.900	406	4	$0.99 \pm 0.50$	3921	20	$0.51 \pm 0.11$
10.75	3.200	1622	2	$0.12 \pm 0.09$	10541	10	$0.09 \pm 0.03$
10.75	3.500	884	1	$0.11 \pm 0.11$	12972	4	$0.03 \pm 0.02$
10.75	3.800	64	0	0	1615	2	$0.12 \pm 0.09$
10.75	all colors	3179	11	$0.35 \pm 0.10$	32440	85	$0.26 \pm 0.03$
11.00	2.075	1	0	0	11	0	0
11.00	2.375	5	0	0	104	2	$1.92 \pm 1.37$
11.00	2.675	16	0	0	536	9	$1.68 \pm 0.56$
11.00	2.975	113	1	$0.88 \pm 0.89$	1449	7	$0.48 \pm 0.18$
11.00	3.275	801	3	$0.37 \pm 0.22$	6078	9	$0.15 \pm 0.05$
11.00	3.575	425	0	0	7530	1	$0.01 \pm 0.01$
11.00	3.875	44	0	0	904	0	0
11.00	all colors	1405	4	$0.28 \pm 0.14$	16614	28	$0.17 \pm 0.03$
11.25	2.450	0	0	0	12	1	$8.33 \pm 8.67$
11.25	2.750	2	0	0	33	0	0
11.25	3.050	6	0	0	186	1	$0.54 \pm 0.54$

TABLE 2 — *Continued*

Lower Left Bin <sup>a</sup>		Faint Sample			Luminous Sample		
$\log(M_*/M_\odot)$	$(u-z)'$	$N_{\text{gal}}$	$N_{\text{AGN}}$	BL AGN %	$N_{\text{gal}}$	$N_{\text{AGN}}$	BL AGN %
11.25	3.350	207	0	0	1769	1	$0.06 \pm 0.06$
11.25	3.650	101	0	0	2453	2	$0.08 \pm 0.06$
11.25	3.950	14	0	0	280	0	0
11.25	all colors	330	0	0	4737	5	$0.11 \pm 0.05$
11.50	3.125	0	0	0	9	0	0
11.50	3.425	24	0	0	277	0	0
11.50	3.725	8	0	0	357	0	0
11.50	4.025	1	0	0	62	0	0
11.50	all colors	33	0	0	708	0	0

<sup>a</sup> Columns of  $\log(M_*/M_\odot)$  and  $(u-z)'$  give the values associated with the lower left corner of each color-mass bin, as shown in Figures 11 and 12. Bins are 0.25 dex wide in mass and 0.3 dex high in color, and bins with less than five inactive galaxies are not shown. Rows with “all colors” give the numbers and fraction of broad-line AGNs in that entire mass slice.